Molecular Dynamics Simulation of Conformational Change of Poly(Ala-Gly) from Silk I to Silk II in Relation to Fiber Formation Mechanism of *Bombyx mori* Silk Fibroin

Tsutomu Yamane, Kôsuke Umemura, Yasumoto Nakazawa, and Tetsuo Asakura*

Department of Biotechnology, Tokyo University of Agriculture and Technology, Koganei, Tokyo 184-8588. Japan

Received April 12, 2003; Revised Manuscript Received June 11, 2003

ABSTRACT: The fiber formation mechanism of *Bombyx mori* silk fibroin by silkworm is essentially the structural change from silk I (the silk fibroin structure before spinning in the solid state) to silk II (the silk fibroin structure after spinning) under external forces in both silk gland and spinneret of *B. mori* silkworm. Recently, we proposed structural models for silk I and silk II forms of the model peptide $(Ala\text{-}Gly)_{15}$ of *B. mori* silk fibroin using mainly solid-state NMR methods. In this paper, molecular dynamics (MD) calculation was performed to simulate the structural change of poly(Ala-Gly) from silk I to silk II and to clarify the detailed mechanism of the silk fiber formation. The silk I structure (repeated β-turn type II) changes to silk II structure (heterogeneous structure, but mainly antiparallel β-sheet) by stretching of the chain with MD simulation, but the change occurs only under very high temperature such as 1000 K and large tensile stress (1.0 GPa). However, the structural change during the MD simulation occurs more easily by taking into account several external forces (the presence of water molecules around the silk chains, and application of both shear and tensile stresses to the silk fibroin) applied to the silk fibroin simultaneously. The heterogeneous structure of the silk fiber determined previously with solid-state NMR could be reproduced well with the MD calculation and then molecular mechanics calculation after removal of water molecules.

Introduction

Silk fibroin from the *Bombyx mori* silkworm is an Ala/Gly-rich protein, which is spun from aqueous solution at room temperature to produce strong and tough fibers.[1] Synthetic materials with comparable properties must be processed at much higher temperatures and/or from less benign solvents. Hence, it is most intriguing to resolve the molecular conformation of silk fibroin before and after spinning and the mechanism of the structural transition during fiber formation in developing new silklike fibers.

B. mori silk fibroin can assume two distinct structures in the solid state, namely silk I before spinning, and silk II after spinning, that is, the silk fiber.[2] Most recently, we have resolved the molecular conformation of silk I as a "repeated β-turn type II", using solid-state NMR methods such as 2D spin diffusion NMR under off magic angle spinning, Rotational echo double resonance (REDOR) and ^{13}C chemical shift data as well as the X-ray diffraction data of poly(Ala-Gly) sample in silk I form are shown in Figure 1.[3,4] To examine the favorable secondary structure(s) associated with silk fibroin molecules, we analyzed the results of molecular dynamic (MD) simulations of three model dipeptides of the type Ac−Xxx−NHMe, (where Xxx = Gly, Ala, and Ser), in *explicit* water because the silk fibroin before spinning in the silk gland is in water.[5] The conformational probability maps constructed for these dipeptides indicate that the torsion angles of Gly, Ala, and Ser residues in the type II β-turn structure are in the stable state even in water, and only our model among silk I models proposed previously can satisfy the stable state for these residues simultaneously. The high possibility of the appearance of β-turn structure is pointed out by the MD simulation of single Ac−$(Ala\text{-}Gly)_8$−NHMe molecule in water.[5]

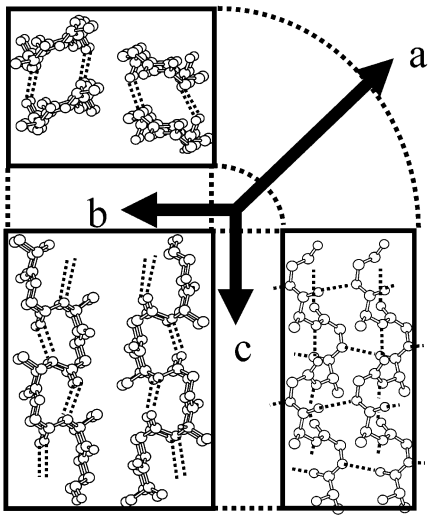

Figure 1. Crystal structure of *B. mori* silk fibroin in a silk I form proposed previously.[3] A repeat β-turn type II structure, stabilized by a 4→1 *intra*molecular hydrogen bond, was proposed. The overall planar sheets were held together by a number of *inter*molecular hydrogen bonding interactions, involving the "central amide-bond" of the β-turn, perpendicular to *intra*molecular interactions.

Moreover, ^{13}C solid-state NMR has also been applied to clarify the heterogeneous structure of the natural fiber from *B. mori* silk fibroin in the silk II form.[6] Figure 2 shows the expanded ^{13}C CP/MAS NMR spectrum of Ala Cβ carbon of the crystalline fraction (56% of total silk fibroin and mainly $(Ala\text{-}Gly\text{-}Ser\text{-}Gly\text{-}Ala\text{-}Gly)_n$ sequences).[7] The peak was broad and asymmetric. The

* To whom correspondence should be addressed. Telephone and Fax: +81−42−383−7733.

10.1021/ma034466o CCC: $25.00
Published on Web 08/06/2003

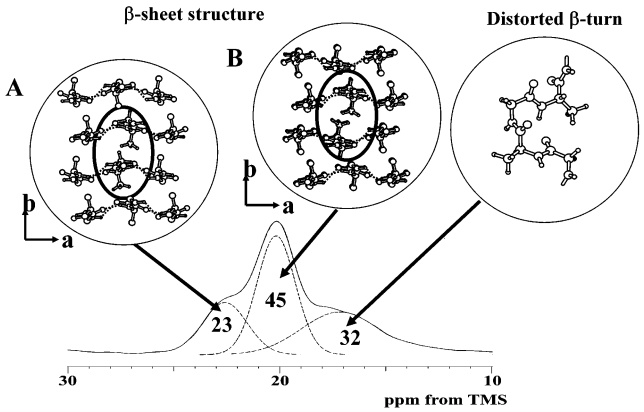

Figure 2. Heterogeneous structure of the crystalline fraction of *B. mori* silk fibroin in a silk II form reported previously.[7] The detailed ^{13}C CP/MAS NMR analysis of the asymmetric Cβ peak of Ala residue of $(AG)_{15}$ in a silk II form clarified that the structure was heterogeneous; a mixture of 23% β-sheet (A; all methyl groups of Ala residues point toward the same direction), 45% β-sheet (B; all methyl groups of Ala residues alternatively point to opposite directions) and 32% distorted β-turn structures.

relative proportions of the various heterogeneous components were determined from their relative peak intensities after line shape deconvolution: 32% distorted β-turn, 23% β-sheet (parallel Ala residues) and 45% β-sheet (alternating Ala residues).[7] The remaining fraction, 44% of total silk fibroin was also analyzed with ^{13}C CP/MAS NMR.[8] The fraction was considered as an amorphous Tyr-rich region which consists of 22% distorted β-turn and 22% distorted β-sheet. It is concluded that the structural change from silk I to silk II occurs mainly for the sequence $(Ala\text{-}Gly\text{-}Ser\text{-}Gly\text{-}Ala\text{-}Gly)_n$ in *B. mori* silk fibroin. Thus, on the basis of determination of the detailed structures in both silk I and silk II forms, it is possible to discuss the mechanism of the structural transition during fiber formation. It may be noted that the concentration of the silk fibroin before spinning, stored in the middle silk gland, is about 30% in water.[9] Magoshi et al.[10] and Kataoka et al.[11−15] described that the soluble silk in the gland and spinneret of *B. mori* silkworm undergoes a conformational change under tensile and shear stresses and loss of water.

In this paper, to clarify the mechanism of the conformational change from silk I to silk II, that is, the fiber formation mechanism, the MD simulation was performed by taking into account external forces applied to the silk fibroin in both silk gland and spinneret. Namely, the presence and loss of water and tensile and shear stresses are considered to be the external forces.

Methodology

In this study, several series of MD and molecular mechanics (MM) calculations were carried out by using the "Discover 3" module in Insight II (4.0.0 P+, Accelrys Inc.) on an OCTANE workstation (Silicon Graphics Inc.). All of the calculations and preparation for initial structures were performed by using some of the module in Insight II.

1. Molecular Dynamics Calculation under Tensile Stress in Vacuo or in Water. As the initial arrangement of the chains in an in vacuo system, four $(Ala\text{-}Gly)_4$ chains with repeated β-turn type II forms were set according to the cell system reported in previous papers.[3,16] To simulate the infinite bulk system of the infinite repeated polymer chains, a periodic boundary condition, where N- and C-terminal were connected to mirror image of themselves, was used. Next, four $(Ala\text{-}Gly)_4$ molecules embedded in water molecules were used for the initial arrangement of the chains in an aqueous solution system. The periodic cell contained 229 water molecules, which corresponds to the concentration of silk fibroin in the middle silk gland (about 30 w/v%). The preparation of the system is as follows. Four $(Ala\text{-}Gly)_4$ chains with repeated β-turn type II forms were placed in a periodic boundary cell homogeneously by using "crystal cell" module in Insight II and then water molecules were introduced by using "soak" option in Insight II. In these initial structures in vacuo and in aqueous solution systems, silk fibroin and water molecules are not in the equilibrium state. The MD simulations were continued until reaching the equilibrium state under nonstress condition, which is described as the "equilibrium stage" in the latter part of this section. The Parrinello and Rahman method[17] was used for MD simulation under external stress such as tensile and/or shear stress. In this method, cell vectors ($\boldsymbol{a}$, $\boldsymbol{b}$, $\boldsymbol{c}$), which determine the cell shape and size, are introduced as a degree of freedom in the system. Then, the Lagrangians of the system at the nth time step in a simulation are modified based on before an $(n-1)$th time step with a term representing the kinetic energy of the cell:

$$L_n = \frac{1}{2}\sum_{i=1}^{N} m_i \dot{s}'_{i,n} G_n \dot{s}_{i,n} - \sum_i^N \sum_j^N \phi(|r_{i,n} - r_{j,n}|) + \frac{1}{2} W \,\mathrm{Tr}(\boldsymbol{h}'_n \dot{\boldsymbol{h}}_n) - p(\Omega_n - \Omega_{n-1}) + \Omega_{n-1}\mathrm{Tr}(\boldsymbol{\sigma} - p)\epsilon_n \quad (1)$$

Here, m_i, $\boldsymbol{s}_{i,n}$ are mass and positional parameters for the ith atom in the cell at the nth time step. $\boldsymbol{h_n} = \{\boldsymbol{a_n}, \boldsymbol{b_n}, \boldsymbol{c_n}\}$is the cell vector matrix at the nth time step, $\mathbf{G_n} = \boldsymbol{h}'_n \boldsymbol{h_n}$, $\boldsymbol{r}_{i,n} = \boldsymbol{h_n} \boldsymbol{s}_{i,n}$, ϕ is the interaction potential, and W is an arbitrary variable which is defined by the user (here, we used the default value). p and Ω_n are the pressure and volume of the cell, respectively. $\boldsymbol{\sigma}$ and ϵ are stress and strain tensors, respectively. The dots above symbols indicate time derivatives, and primes indicate matrix transposition. Tr is the trace of a matrix. Both the shape and the volume of the cell can change, and therefore, the internal stress of the system can be set to match the externally applied stress $\boldsymbol{\sigma}$. In this study, we performed six series of MD simulations under different tensile stress which was set parallel to the fiber axis; the fiber axis was defined as z axis of Cartesian coordinate of the system and σ_{zz} term in the stress tensor $\boldsymbol{\sigma}$ was set to be 0.0, 0.2, 0.4, 0.6, 0.8, and 1 GPa. In both cases, in vacuo and in water, the velocity Velret algorithm was used to integrate Newton's equation of motion (with a time step of 1.0 fs).[18] Temperature of the systems was controlled by Andersen method[19] at 1000 K (in vacuo system) and 298 K (in aqueous solution system). The conformational change during MD simulation does not occur at lower temperature in the in vacuo system under smaller tensile stress. For example, after the MD simulation of the system at 600 K even under 1 GPa of tensile stress, several conformational regions other than the C_5 region still remain in the Ramachandran map, meaning that the conformational change is not enough under this condition (data not shown). The processes of MD calculations were the following: initially performed without any external forces until the system

reaches the equilibrium state (equilibrium stage; 5000 steps) and then the calculations continued under tensile stress (simulation stage; 200 000 steps, that is, 200 ps). The snapshot structures were sampled every 20 steps during the latter steps from 101 to 200 ps in simulation stage. All of the simulations were performed by using a pcff force field (Accelrys Inc.). Nonbonded interactions were calculated using a 9.5 Å cutoff distance.

2. Molecular Dynamics Calculation under Both Tensile and Shear Stresses in Water and Then Molecular Mechanics Calculation after Removal of Water. The shear stress applied to the silk fibroin at press part of the spinneret in *B. mori* silkworm has been emphasized.[10−15] Similarly, the shear stress was applied by a stress tensor in the Parrinello and Rahman method.[17] Generally, to introduce the shear stress to the system, nondiagonal terms of stress tensor $\boldsymbol{\sigma}$ (σ_{xy}, σ_{yx}, σ_{yz}, σ_{zy}, σ_{zx}, and σ_{xz}) should be set to nonzero values. However, such a nondiagonal stress tensor causes a change in the shape of the cell largely because such stresses add asymmetrical forces to the cell, and the total energies of the system diverge before reaching equilibrium of the system. On the other hand, diagonal terms of the stress tensor (σ_{xx}, σ_{yy}, and σ_{zz}) add symmetrical forces to the cell, and hence MD simulation under such stresses is more stable. As described above, the control of the stress control method in this study is performed by changing the volume and shape of the cell, so that the internal stress of the system can match the external stress. In other words, strain tensor ϵ in eq 1 is defined as $(h'_{n-1}{}^{-1}\mathbf{G}h_{n-1}{}^{-1} - 1)/2$, which means that diagonal matrix of applied stress tensor σ gives nonzero diagonal and nondiagonal terms of strain tensor to the system. Therefore, we applied shear stress by setting diagonal terms of the stress tensor $\boldsymbol{\sigma}$ as nonzero values. In the present study, we performed four series of MD simulation: (σ_{xx}, σ_{yy}, σ_{zz}) = (−0.3 GPa, −0.3 GPa, 0.1 GPa), (−0.5 GPa, −0.5 GPa, 0.1 GPa), (−0.7 GPa, −0.7 GPa, 0.1 GPa), and (−1.0 GPa, −1.0 GPa, 0.1 GPa). Here, the minus value means that press stress is applied to the cell. These simulations may emphasize the effects of shear stress by applying press stress perpendicular to the fiber axis. In this study, σ_{xx} and σ_{yy} terms are called "shear" stress, and the σ_{zz} term is called "tensile" stress for convenience. Sixteen $(Ala\text{-}Gly)_6$ chains with repeated β-turn type II forms, where N- and C-terminal were connected to mirror image of themselves, were arranged in a periodic cell. The chains are embedded in 916 water molecules for the initial arrangement of the chains in aqueous solution systems, which corresponds to the concentration of silk fibroin in the middle silk gland (about 30 w/v%). The preparation method of this structure is same as that described in the previous part of the Methodology section. To simulate the infinite bulk system of infinite repeated polymer chains, periodic boundary conditions were also used. The temperature of the systems was controlled by the Andersen method[19] at 298 K. The processes of MD calculations are the same as that described in previous part of the Methodology section. The 100 structures, which were sampled every 20 steps during the latter steps from 101 to 200 ps in the simulation stage, were selected after the MD calculation of the system under both tensile and shear stresses in the presence of water, and then the molecular mechanics (MM) calculations were performed after removal of water molecules.

3. Conformational Probability Calculation. The conformational probability distributions of the Ala and Gly residues in $(Ala\text{-}Gly)_n$ chains were calculated at the equilibrium stage and after MD calculations under external forces. Backbone torsion angles of each residue, Ala(ϕ,ψ) and Gly(ϕ,ψ), were extracted from the trajectory of each simulation and used for the calculation of preparing the histograms of conformations $N(\phi \pm 10°,\psi \pm 10°)$. Here $N(\phi \pm 10°,\psi \pm 10°)$ means the number of conformers with torsion angles: $(\phi \pm 10°,\psi \pm 10°)$. The conformational probability $P(\phi,\psi)$ of Ala and Gly residues was calculated according to the following equation[20]

$$P(\phi,\psi) = \frac{N(\phi \pm 10°,\psi \pm 10°)}{N_{\text{total}}} \qquad (2)$$

where N_{total} means the total number of conformations of Ala or Gly residues in the trajectory. The conformational probabilities $P(\phi,\psi)$ were plotted against the torsion angles, ϕ and ψ.

Results and Discussion

1. Conformational Probability Distributions of Ala and Gly Residues in Four $(Ala\text{-}Gly)_4$ Molecules in Vacuo under Tensile Stress. Figure 3 shows Ramachandran plots of the conformational probability distributions of Ala (left) and Gly (right) residues in $(Ala\text{-}Gly)_4$ chains drawn from trajectories of a series of MD simulation in vacuo by changing the tensile stress. There are three local minimum regions: $C7^{ax}$:(ϕ,ψ) = (60°,−70°), α_R:(ϕ,ψ) = (−60°,−60°), and the region ($C7^{eq}$ (ϕ,ψ) = (−60°,60°) plus P_{II} (ϕ,ψ) = (−60°,130°) in the Ramachandran map of Ala residue with no tensile stress.[21] The conformations, $C7^{eq}$ ((ϕ,ψ) = (−60°,60°)) and $C7^{ax}$ ((ϕ,ψ) = (60°,−70°)) have been reported as predominant ones for the Ala residue in vacuo.[20] The $C7^{eq}$ and P_{II} regions tend to separate under 0.2 GPa of tensile stress. With increasing tensile stress, the local minima tend to shift to the corners of the map. This means that the conformation of $(Ala\text{-}Gly)_4$ chain changes from repeated β-turn type II to β-sheet. In addition, the regions of the conformations, $C7^{eq}$, $C7^{ax}$, and α_R, become smaller. Under more than 0.6 Gpa of the tensile stress, the region of preferred conformation is shifted from P_{II} region to the corners. Finally the C_5 region ((ϕ,ψ) = (−150°,150°)) becomes dominant although another small minimum region at around ((ϕ,ψ) = (60°,150°)) appears. On the other hand, there are two major local minimum regions, $C7^{eq}$ and $C7^{ax}$ for Gly residue under no tensile stress as shown in Figure 3. With increasing the tensile stress, both $C7^{eq}$ and $C7^{ax}$ regions become smaller. Under larger tensile stress, the C_5 region becomes dominant.

In general, high conformational flexibility of macromolecules is important to cause the conformational transition. However, the presence of inter- and intramolecular hydrogen bondings in the silk I form restrains the molecular motions. In vacuo system, high kinetic energy, enough to cancel out the hydrogen bonding energy was given by setting the system at high temperature (1000 K). In Figure 3, the local minimum regions in the conformational probability maps are relatively shallower than those in Figure 4 and the conformers with high kinetic energy are jumping around all over the conformational space. Recently, Koyama et al. attempted MD simulation of the crystallization

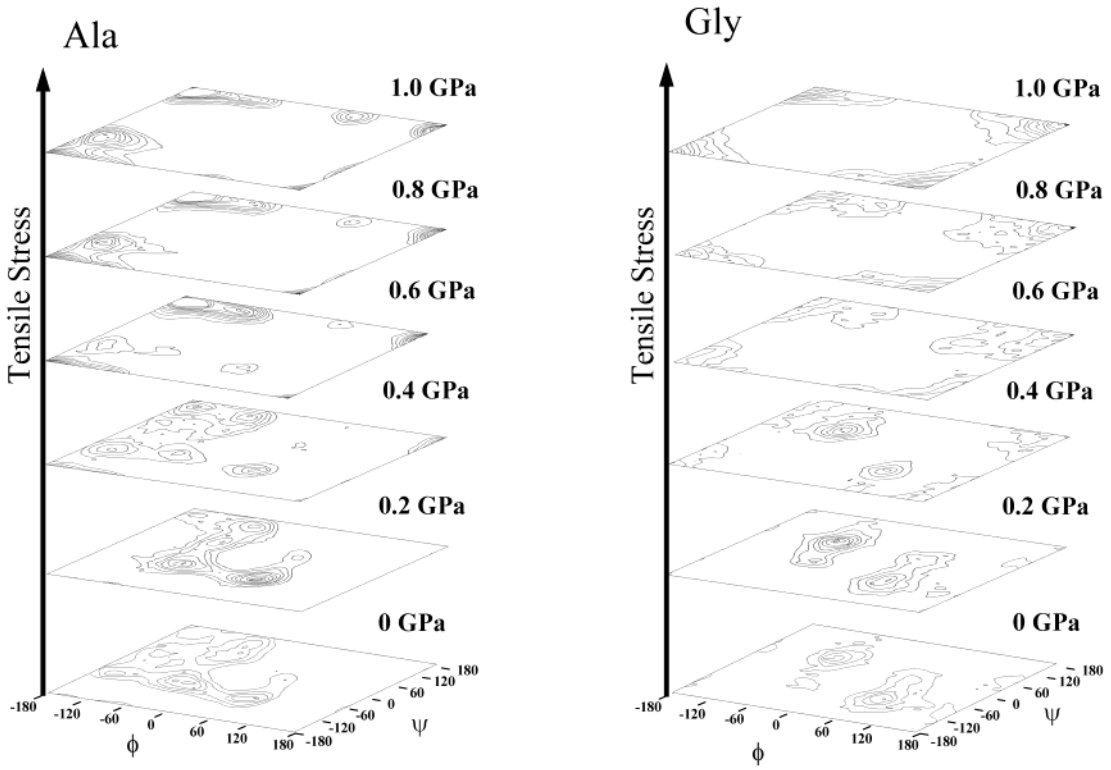

Figure 3. Conformational probability maps of Ala and Gly residues in four $(Ala\text{-}Gly)_4$ chains in vacuo obtained from MD simulation by changing the tensile stress (0, 0.2, 0.4, 0.6, 0.8, and 1.0 GPa). Contour lines of its probability are drawn every 0.0005 from 0.0005 to 0.002.

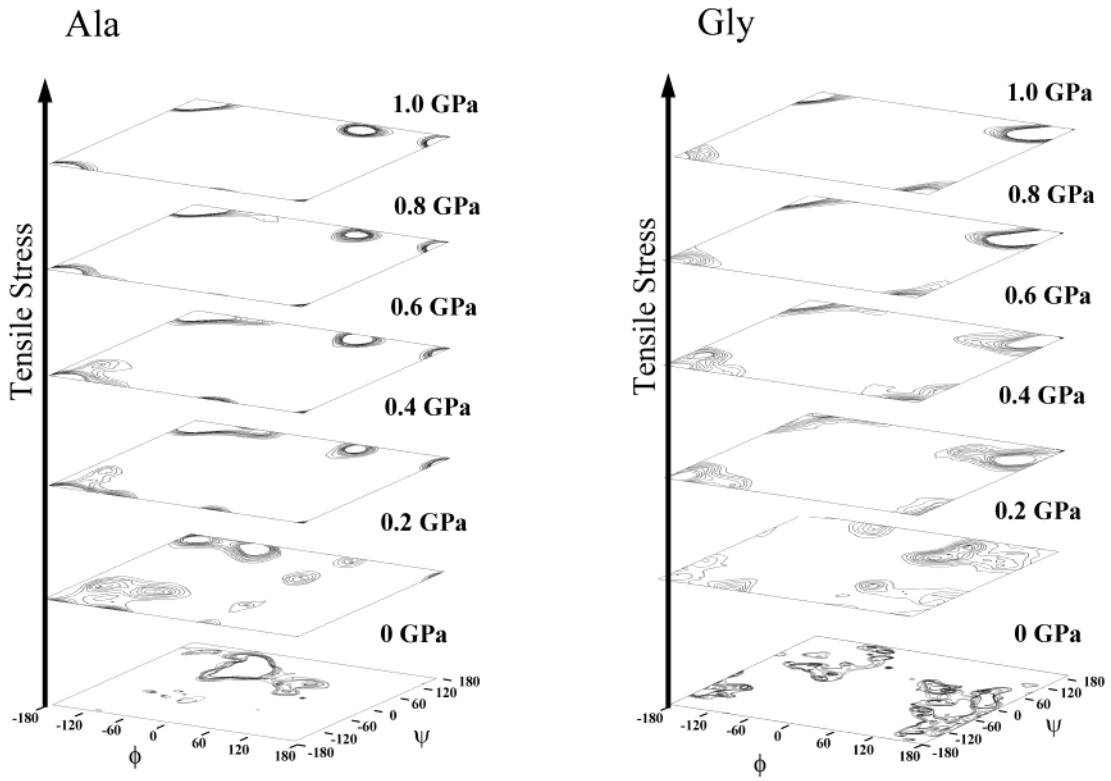

Figure 4. Conformational probability maps of Ala and Gly residues in four $(Ala\text{-}Gly)_4$ chains obtained form MD simulation in aqueous solution by changing the tensile stress (0, 0.2, 0.4, 0.6, 0.8, and 1.0 GPa). Contour lines of its probability are drawn every 0.0005 from 0.0005 to 0.002.

process from oriented amorphous polyethylene, which has no hydrogen-bonding site.[22] The MD simulation for such crystallization process was performed at 330 K for periodic boundary cells containing polyethylene molecules with no solvent molecules. The temperature is quite low compared with our simulation.

2. Conformational Probability Distributions of Ala and Gly Residues in Four $(Ala\text{-}Gly)_4$ Molecules

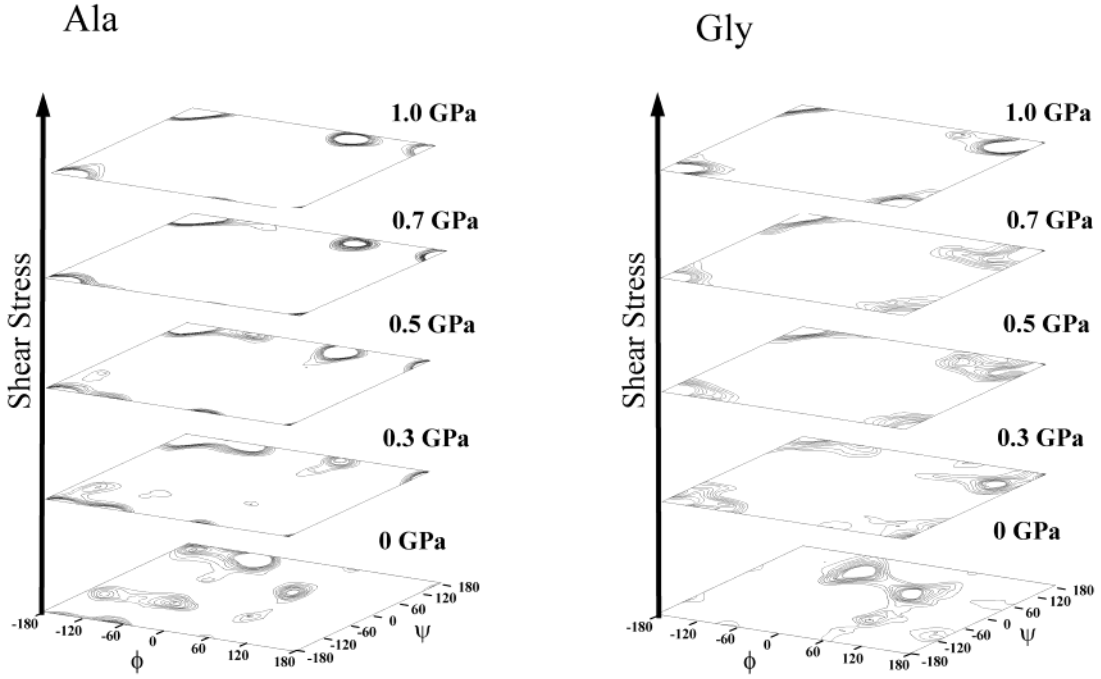

Figure 5. Conformational probability maps of Ala and Gly residues in 16 $(Ala\text{-}Gly)_6$ chains in aqueous solution obtained form MD simulation under 0.1 GPa of the tensile stress by changing the shear stress (0, 0.3, 0.5, 0.7, and 1.0 GPa). Contour lines of its probability are drawn every 0.0005 from 0.0005 to 0.002.

in Water under Tensile Stress. Before application of the tensile stress to the $(Ala\text{-}Gly)_4$ system, which is the equilibrium stage, four $(Ala\text{-}Gly)_4$ chains with β-turn type II forms in aqueous solution were annealed at room temperature. In this process, the intra- and intermolecular hydrogen bondings are weakened and partially destroyed by the presence of water molecules, which causes flexibility of the silk fibroin chains. Then the MD simulation is started under several tensile stresses. Figure 4 shows Ramachandran maps of the conformational probability distributions of Ala and Gly residues in four $(Ala\text{-}Gly)_4$ molecules in water by the MD simulation under different tensile stresses. The conformational changes occur although the temperature is considerably low, 298 K (in aqueous solution system), compared with that in vacuo, 1000 K. It is noted that change of the preferred conformation to the C_5 conformation occurs under weaker stress compared with the MD simulation in vacuo. Thus, the presence of water molecules in the system also destroys the intra- and intermolecular hydrogen bondings of $(Ala\text{-}Gly)_4$ chains under the MD simulation process and leads the conformational changes of $(Ala\text{-}Gly)_4$ molecules easily. There is one small minimum region at around $((\phi,\psi) = (60°,150°))$ in the map of the Ala residue as well as the case of the in vacuo calculation.

3. Conformational Probability Distributions of Ala and Gly Residues in 16 $(Ala\text{-}Gly)_6$ Molecules in Water under Both Shear Stress and Weak Tensile Stress. The conformational change of the Ala and Gly residues of 16 $(Ala\text{-}Gly)_6$ molecules embedded in water molecules during the MD simulation was examined under both shear stress and weak tensile stresses. This seems close to the real system where the external forces are applied to the silk fibroin in water in *B. mori* silkworm. However, it is difficult to measure the values of both tensile and shear stresses in the silkworm. Therefore, the MD calculation was tried by changing the shear stress when the tensile stress is fixed to be 0.1 GPa because the presence of strong shear stress applied to the silk fibroin at the press part of the spinneret has been emphasized. The Ramachandran maps of the conformational probability distributions for Ala and Gly residues were shown as a function of shear stress in Figure 5. The change of the preferred conformation to C_5 conformation occurs with increasing the shear stress. This is a similar tendency to the change in the conformational maps in water under only tensile stress. Moreover, the conformational probability maps without tensile or shear stress in Figures 4 and 5 suggest that silk I (Ala, $(\phi,\psi) = (-60°,130°)$, and Gly, $(\phi,\psi) = (70°,30°)$) is a relatively stable structure in aqueous solution, which has been discussed in our previous paper from the standpoint of stability of Ala and Gly residues in aqueous solution.[5]

The time dependences of the conformational probability distributions for Ala and Gly residues in the aqueous solution system were shown when the shear stress is 0.7 GPa and the tensile stress is 0.1 GPa in Figure 6. The conformational maps at the equilibrium stages are the same as those in Figure 4 (0 GPa). Under the stress, the conformation changes with time and the preferred conformation becomes mainly a C_5 conformation for both residues at 80−82 ps although there is also one small minimum region at around $((\phi,\psi) = (60°,150°))$ in the map of Ala residue. It is interesting to examine the conformational change of $(Ala\text{-}Gly)_6$ molecules in the aqueous solution system with time under the stress in relation to the fiber formation process. At the equilibrium stage of Ala residue, there are two stable regions where we call as Ala-1 ($-60° < \phi < 0°$, $0° < \psi < 180°$) and Ala-2 ($0° < \phi < 120°$, $0° < \psi < 60°$) in this study. Over 0−2 ps, both regions, Ala-1 and Ala-2, are divided into a number of the stable regions. However, Ala-1 region tends to shift toward P_{II} region. Over 10−12 ps, the Ala-1 region then shifts toward the C_5 region. and most of the stable regions shift to the nearest corner over 80−82 ps. Namely, most of the Ala residues form

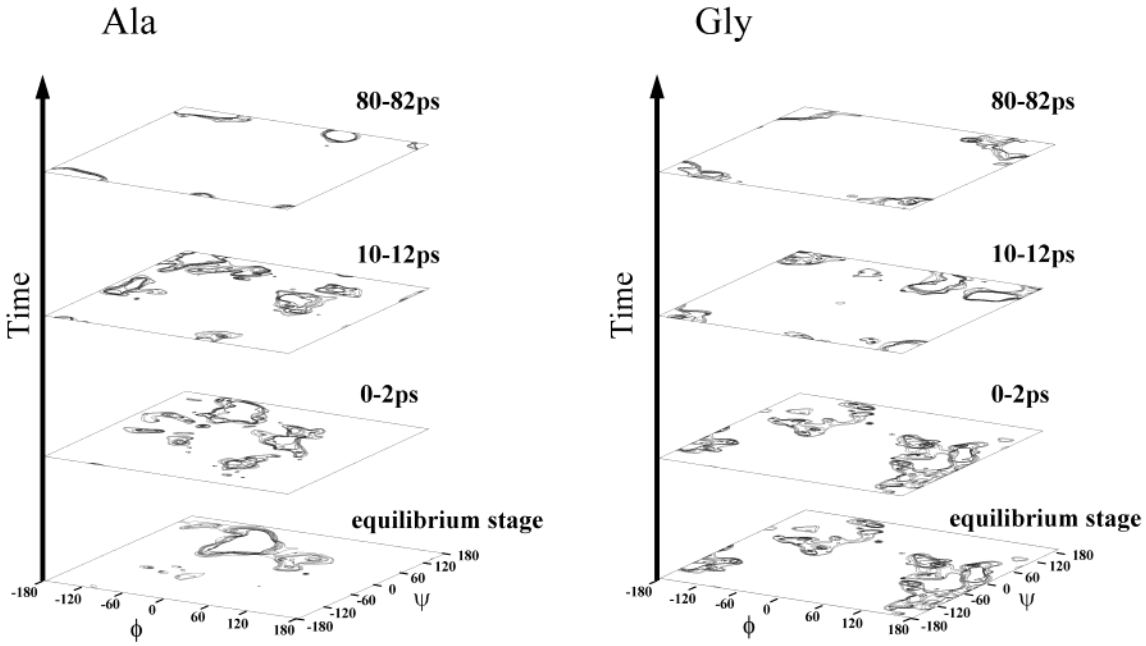

Figure 6. Conformational probability maps of Ala and Gly residues in 16 $(Ala\text{-}Gly)_6$ chains in aqueous solution obtained form MD simulation under 0.1 GPa of the tensile stress and 0.7 GPa of the shear stress with time. Contour lines of its probability are drawn every 0.0005 from 0.0005 to 0.002.

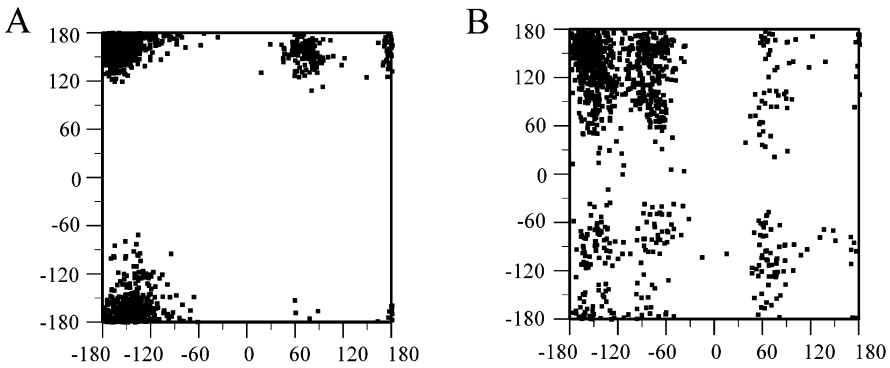

Figure 7. Conformational distribution, A, of Ala residues in 16 $(Ala\text{-}Gly)_6$ chains in aqueous solution obtained form MD simulation under 0.1 GPa of the tensile stress and 0.7 GPa of the shear stress, and then the distribution, B, calculated with molecular mechanics method after removal of water molecules.

β-sheet conformation with another one region, around $(\phi,\psi) = (60°,150°)$. On the other hand, the conformation of Gly residue spreads over the Ramachandran plot during equilibrium stage because of high flexibility. For convenience, these are classified into four regions: Gly-1 ($-120° < \phi < 0°$, $0° < \psi < 180°$), Gly-2 ($60° < \phi < 120°$, $0° < \psi < 60°$), Gly-3 ($120° < \phi < 180°$, $0° < \psi < 120°$) and Gly-4 (($60° < \phi < 180°$, $-180° < \psi < 0°$) and ($-180° < \phi < -120°$, $-150° < \psi < -60°$)). Over 0−2 ps, the conformational distribution on Ramachandran plot is mostly the same as that at the equilibrium stage. Over 10−12 ps, Gly-1 and Gly-4 regions tend to shift to the nearest corners, which means that they converge to a C_5 conformation. At the same time, Gly-2 and Gly-3 regions shift to the upper side by rotation of the ψ angle. In this stage, the shifted Gly-2 region, $(\phi,\psi) = (60°, 150°)$, is the same region of the Ala residue that appeared over 80−82 ps. Finally, the most of the stable regions shift to nearest corner over 80−82 ps, which means the Gly residues form the β-sheet conformation completely.

4. Conformational Distributions of Ala Residues in $(Ala\text{-}Gly)_6$ Molecules after Removal of Water. After MD simulation under 0.7 GPa of shear stress and 0.1 GPa of weak tensile stress, the conformations of Ala residues are plotted in Figure 7A, where water molecules are present. This is the same data from Figure 5 (at 0.7 GPa of shear stress), but the data are shown without the conformational probability calculation. Then the water molecules are removed and MM calculation was performed by taking into account the experimental results; the water molecules are rapidly evaporated just after the spinning of the silkworms.[15] After this treatment, the conformational change in the Ramachandran map of Ala residue is remarkable as shown in Figure 7B. The scattering of the conformations in the map becomes larger. The C_5 and P_{II} regions tend to appear separately. In addition, one small minimum region at around ($(\phi,\psi) = (60°,150°)$) in Figure 7A tends to disappear because of the dispersion.

In our previous papers,[7,8] we reported that *B. mori* silk fiber takes a heterogeneous structure. Namely, as shown in Figure 2, the crystalline fraction (mainly repeated Ala-Gly-Ser-Gly-Ala-Gly sequences) takes 27% β-sheet (parallel Ala residues), 46% β-sheet (alternating Ala residues), and 27% distorted β-turn. Thus, we will try to check whether the heterogeneous structure could be reproduced by this calculation. By considering the

Table 1. Fraction of β-Sheet and β-Turn Calculated for Ala Residues in 16 $(Ala\text{-}Gly)_8$ Chains with MD Simulation Obtained by Changing the Shear Stress under 0.1 GPa of the Tensile Stress[a]

	fraction of β-sheet (%)	fraction of β-turn (%)
MD simulation (1.0 GPa)	75.9	24.1
MD simulation (0.7 GPa)	72.7	27.3
MD simulation (0.5 GPa)	74.9	25.1
experiment	73.0	27.0

[a] Details are denoted in the text.

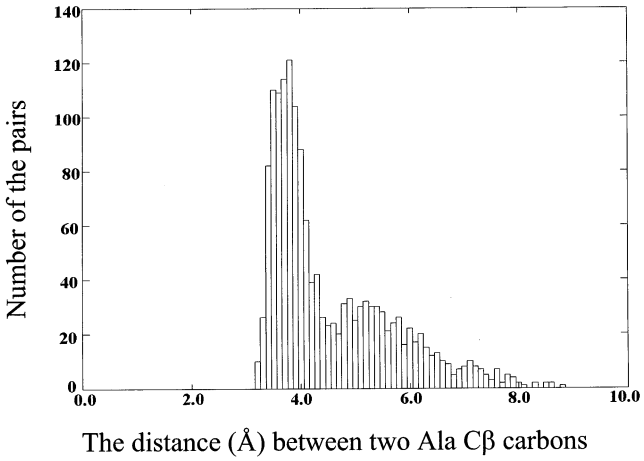

Figure 8. Number of Ala Cβ carbon pairs with the distance (less than 10 Å) between two Cβ carbons of Ala residues in the region of β-sheet (ϕ and $\psi = -150° \pm 30°$, $150° \pm 30°$) plotted against the distance. These pairs are selected from Figure 7B. Details are described in the text.

distribution around the torsion angles corresponding two minima, β-sheet and β-turn, the fractions of β-sheet (ϕ and $\psi = -150° \pm 30°$, $150° \pm 30°$) and β-turn (ϕ and $\psi = -60° \pm 40°$, $130° \pm 40°$) are calculated and summarized in Table 1 by changing the shear stress. The experimental value of the fraction is 73% (β-sheet) and 27% (β-turn), which could be reproduced by the calculation (0.7 GPa).

Next, we examined the observed relative intensities of two intermolecular arrangements of antiparallel β-sheet structure, that is, 27% β-sheet (parallel Ala residues) and 46% β-sheet (alternating Ala residues) in the Cp fraction. For the Ala residues in the region of β-sheet (ϕ and $\psi = -150° \pm 30°$, $150° \pm 30°$), all distances between two Cβ carbons among these Ala residues were calculated except for the distances between two Ala Cβ carbons within one chain. The number of the pairs with the distance less than 10 Å under 0.7 GPa of the shear stress was plotted against the distance as shown in Figure 8. There are two peaks centered at around 4 and around 5 Å although the latter peak is broad. These distances of two Ala Cβ carbons calculated here coincide with the distances of two Ala Cβ carbons in the cases B and A in the circles of Figure 2, respectively.[23] The fraction of the peak centered at 4 Å is larger than that centered at 5 Å, which is also in agreement with the NMR result (Figure 2). Thus, the heterogeneous structure determined from ^{13}C CP/MAS NMR spectrum of the Cp fraction could be reproduced from the calculation.

Silk fibroin fiber has outstanding mechanical properties despite being spun at room temperature and from aqueous solution by silkworms. Now we are trying to determine detailed three-dimensional structure of the spinneret containing a pair of silk filaments and chitin plates based on about 1000 optical micrographs of the cross section. The fiber formation mechanism of *B. mori* silk fibroin will be clarified from both information on such real system and the molecular dynamics (MD) calculation of the structural change of Poly(Ala-Gly) from silk I to silk II performed in this study.

Acknowledgment. We acknowledge support from the Insect Technology Project, Japan.

References and Notes

(1) O'Brien, J. P.; Stephen, R. F.; Termonia, Y.; Gardner, K. H. *Adv. Mater.* **1998**, *10*, 1185−1195.
(2) Lotz, B.; Cesari, F. C. *Biochimie* **1979**, *61*, 205−214.
(3) Asakura, T.; Ashida, J.; Yamane, T.; Kameda, T.; Nakazawa, Y.; Ohgo, K.; Komatsu, K. *J. Mol. Biol.* **2001**, *306*, 291−305.
(4) Asakura, T.; Yamane, T.; Nakazawa, Y.; Kameda, T.; Ando, K. *Biopolymers* **2001**, *58*, 521−525.
(5) Yamane, T.; Umemura, K.; Asakura, T. *Macromolecules* **2002**, *35*, 8831−8838.
(6) Marsh, R. E.; Corey, R. B.; Pauling, L. *Biochem. Biophys. Acta* **1955**, *16*, 1−34.
(7) Asakura, T.; Yao, J.; Yamane, T.; Umemura, K.; Ulrich, A. S. *J. Am. Chem. Soc.* **2002**, *124*, 8794−8795.
(8) Asakura, T.; Yao, J. *Protein Sci.* **2002**, *11*, 2706−2713.
(9) Asakura, T.; Watanabe, Y.; Ito, T. *Macromolecules* **1984**, *17*, 2421−2426.
(10) Magoshi, J.; Mizuide, M.; Magoshi, Y.; Takahashi, K.; Kubo, M.; Nakamura, S. *J. Polym. Sci., Polym. Phys. Ed.* **1979**, *17*, 515−520.
(11) Magoshi, J.; Magoshi, Y.; Nakamura, S. *J. Appl. Polym. Sci.: Appl. Polym. Symp.* **1985**, *41*, 187−204.
(12) Kataoka, K.; Uematsu, I. *Koubunshi Ronbunshu* **1976**, *33*, 453−462.
(13) Kataoka, K.; Uematsu, I. *Koubunshi Ronbunshu* **1977**, *34*, 7−13.
(14) Kataoka, K.; Uematsu, I. *Koubunshi Ronbunshu* **1977**, *34*, 457−464.
(15) Kataoka, K. *J. Sericul. Sci. Jpn.* **1981**, *50*, 478−483.
(16) Okuyama, K.; Nakajima, Y.; Hasegawa, Y.; Hirabayashi, K.; Nishi, N. *J. Sericul. Sci. Jpn.* **1988**, *57*, 23−30.
(17) Parrinello, M.; Rahman, A. *J. Appl. Phys.* **1981**, *52*, 7182−7190.
(18) Swope, W. C.; Andersen, H. C.; Berens, P. H.; Wilson, K. R. *J. Chem. Phys.* **1982**, *76*, 637−649.
(19) Andersen, H. C. *J. Chem. Phys.* **1980**, *72*, 2384−2393.
(20) Yamane, T.; Inoue, Y.; Sakurai, M. *Chem. Phys. Lett.* **1998**, *291*, 137−142.
(21) Brooks, C. L.; III; Case, D. A. *Chem. Rev.* **1993**, *93*, 2487−2502.
(22) Koyama, A.; Yamamoto, T.; Fukao, K.; Miyamoto, Y. *Phys. Rev. E* **2002**, *65*, 050801(R).
(23) Takahashi, Y.; Gehoh, M.; Yuzuriha, K. *Int. J. Biol. Macromol.* **1999**, *24*, 127−138.

MA034466O